ChemComm

Accepted Manuscript

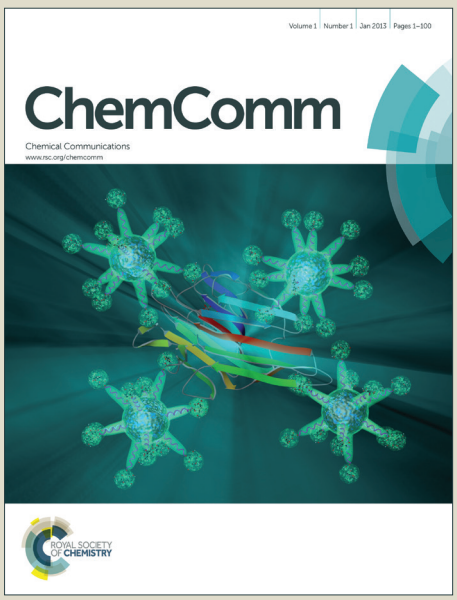

ROYAL SOCIETY OF CHEMISTRY

www.rsc.org/chemcomm

Journal Name

RSCPublishing

COMMUNICATION

Heterostructure of AuAg Nanoparticle Tipping on Ag_2S Quantum Tube

Cite this: DOI: 10.1039/xoxxoooooox

Yang Tian,* Weiwei Zhou, Hanqin Tang, Hongbing Fu, Ligang Wang

Received ooth January 2012,
Accepted ooth January 2012

DOI: 10.1039/xoxxoooooox

www.rsc.org/

We report synthesis of a novel metal-semiconductor heterostructure, in which AuAg alloy nanoparticle locates at Ag_2S quantum tube tip. The Ag_2S quantum tube has an ultrathin wall below 1 nm. The formation mechanism, UV-Vis, luminescence and Photoelectrochemical activity of the prepared heterostructure were further studied.

In recent years, heteronanostructures of metal-semiconductor, in which metal and semiconductor are closely coupled in one nanostructure, have shown novel properties that exceed the functionality of the individual components.[1] For example, charge separation at the metal-semiconductor interface can enhance its photocatalytic activities or modify its nonlinear optical response, and metal tipping on semiconductor nanorods (NRs) can serve as anchor points for electrical connections or for self-assembly into complex structures.[2] These unique properties make them for promising candidates for the design of next generation electronic devices, solar cells, H_2 generation as well as photocatalysis.[3]

Controlling composition and shape of metal-semiconductor heterostructures is important for the fundamental understanding of size- and shape-dependent scaling laws. Studies of metals coupled with semiconductors in different morphologies have been conducted in the past decade. For example, the most-studied heterostructure is co-joined sphere-to-sphere.[4] Metal nanoparticles such as Co, Au and Pt tipping on semiconductor CdSe, CdS and CdS/CdSe NRs have also been reported using both thermal and light-assisted approaches.[5] Heterostructure of Pt cubes tipping on CdS NRs was prepared by Alivisatos' group.[6] In addition, metal nanoparticles coupled with semiconductor nanoplate, hollow-sphere and nanopyramids were also prepared successfully.[7] Despite these excellent advantages, it is extremely desirable to develop more metal-semiconductor heterostructures with tailored morphologies to meet the growing demands for their applications.

Since the discovery of carbon nanotube, inorganic hollow nanotubes have attracted much interest because of their novel properties and potential applications in energy storage, catalysis, and medicine transfer.[8] Considerable advances have been made in the synthesis of metal oxide and chalcogen semiconductor nanotubes.[9] However, the shells of these nanotubes are usually far larger than 10 nm, which hinders their applications related to quantum confinement effect. Monoclinic Ag_2S is a direct and narrow band gap (1.1 eV) semiconductor with a relatively high absorption coefficient and excellent optical limiting properties.[10] Ag_2S has wide applications in optical and electronic devices such as photoconductive cells, infrared detectors and near-infrared (NIR) vivo fluorescence imaging.[11] To this point, many efforts have been devoted to Ag_2S nanostructures such as quantum dots (QDs), nanowires, nanospheres and nanotubes.[12] Based on such studies, heterostructures of metal combined with Ag_2S nanocrystals such as nanoparticles, hollow-spheres, nanoframs, and nanowires, have been achieved. [3f, 3g, 4a, 7b, 12a, 13] However, synthesis of metal nanoparticle tipping on Ag_2S quantum tube (QT) is still limited, which may be caused by the difficulties in synthesis of Ag_2S QTs and the lattice strain between the monoclinic Ag_2S and face-centered cubic (fcc) metals.[4a]

Herein, we report fabricating the novel heterostructure of AuAg alloy nanoparticles locating on Ag_2S QT tips. To our knowlege, it is the first example of metal nanoparticles tipping on semiconductor QTs regradless semiconductor components. More interestingly, the Ag_2S QT in as-prepared heterostructure has an ultrathin shell with thickness of 0.8 ±0.1 nm. We show that first by using ZnS NRs as the starting seeds reacting with $AuCl_3$ to prepare heterostructure of gold tipping on ZnS NRs (defined as HS1, shown in Scheme 1). Secondly, the ZnS NRs in HS1 transformed into Ag_2S QTs with Ag^+ *via* Kirkendall effect, and the gold nanoparticles in HS1 transformed into AuAg alloy nanoparticles during their ripening with Ag^+, resulting in the novel heterostructure of AuAg alloy nanoparticles tipping on Ag_2S QTs (defined as HS2, shown in Scheme 1). The schematic procedure and intermediate mechanism are illustrated in Scheme 1. Furthermore, the UV-visible and photoluminescence (PL) spectra displayed electronic coupling between the AuAg

nanoparticle and Ag_2S QTs. The prepared HS2 product showed effective photoelectrochemical (PEC) catalysis for H_2 evolution reaction.

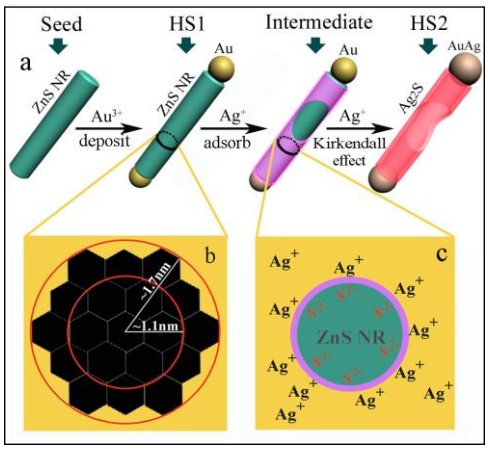

Scheme 1. Schematic illustration of the formation process and mechanism of AuAg-Ag_2S heterostructure(a); cross section of ZnS NR (b); cross section of intermediate transition from HS1 to HS2 (c).

The phase and purity of as-prepared ZnS NRs, HS1 and HS2 products were characterized by powder X-ray diffraction (XRD). Fig. S1 and S2 show the correct XRD patterns of ZnS NRs and HS1. Fig. S3 is the XRD pattern of HS2 product, in which the peaks at 38.2 º, 44.4 º and 64.5 º can be indexed to cubic metal Au (JCPDS No.04-0784) or Ag (JCPDS No.03-0931). However, it is difficult to distinguish metal Au and Ag according to the XRD pattern, because they have nearly the same crystalline structure (fcc) and lattice constant (a = 0.408 nm for Au; a = 0.407 nm for Ag). On the other hand, all of the other peaks in the XRD pattern can be attributed to a monoclinic Ag_2S (JCPDS No. 14-0072). Furthermore, the diffraction peaks of ZnS were rarely detected in the XRD pattern, indicating that the ZnS NR precursor was completely transformed into Ag_2S in HS2.

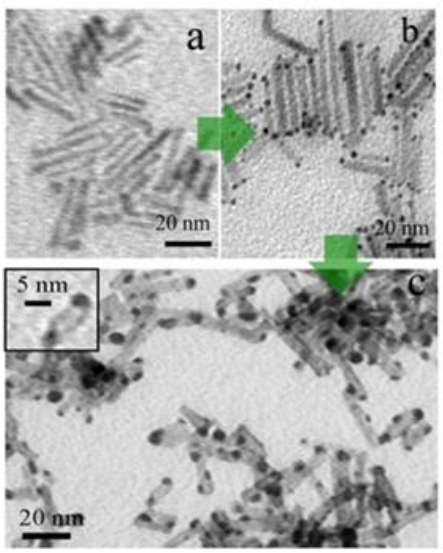

Fig. 1. TEM images of the ZnS NRs (a), HS1 (b) and HS2 (c); the inset is a local magnification.

The morphology and size of the prepared ZnS NR seeds as well as HS1 and HS2 products were examined by transmission electron microscopy (TEM). Fig. 1a is a typical TEM image of a ZnS seed showing the rod-like morphology with a diameter of ~3 nm and a length of 15-40 nm. Fig. 1b is a TEM image of HS1. It shows clearly a heterostructure of gold nanoparticles on the NR tips with little particles on NR sides. The diameter of the gold nanoparticles on the NR tips is ~2 nm. The diameter and length of ZnS NR component in HS1 kept the sizes of the ZnS NR seeds. Fig. 1c is a typical TEM image of the prepared HS2. It shows clearly the heterostructure of nanoparticles tipping on the QTs. The inset of Fig. 1c is a magnification, which verifies the hollow tube in the heterostructure. The diameter of the nanoparticles on the nanotube tips is ~5 nm, which is larger than gold nanoparticles in HS1. The QTs show an outer diameter of approximately 5 nm, larger than that of ZnS NR (~ 3 m); the length of the nanotube is 15 nm to 40 nm, which is similar as ZnS NR. Note that the shell of QT has a thickness of 0.8±0.1 nm. This thickness is close to the single-cell size of monoclinic Ag_2S in the y and z axes (cell parameter b=0.693 nm and c=0.786 nm); or is twice the cell size of the Monoclinic Ag_2S in the x axis (a=0.423 nm). Therefore, the shell of the Ag_2S QT in the heteronanostructure is in thickness of very few atoms.

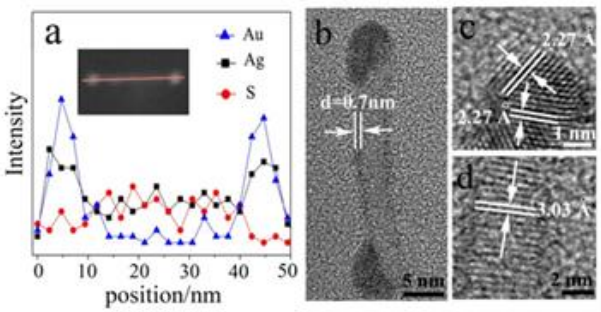

Fig. 2. Elemental line profiles (see the red line in the inset STEM image) (a); HRTEM images of single HS2 (b), AuAg component in HS2(c), and Ag_2S component in HS2 (d)

The heterostructure and local atomic composition of the HS2 were determined based on Energy Dispersive X-Ray Spectroscopy (EDX) line scanning. The red line in the inset of Fig. 2a indicates the scanning path of an electron beam, and a clear presentation of the elemental distribution was derived by plotting the EDX line scan signal versus the distance along the axis of the HS2. Overall, the EDX line scan profile shows that the double peaks of Au and Ag locate at the tips of the heterostructures. The S $K\alpha_1$ and Ag peaks at the middle regions of the EDX line reveal the composition of the Ag_2S QT. High-Resolution TEM (HRTEM) analysis was employed to characterize the intrinsic crystallography of the HS2. The HRTEM image (Fig. 2b) illustrates clearly two nanoparticles located at the tips of a QT. The shell of QT component is ultrathin with a thickness of ~0.7 nm. The AuAg nanoparticle in HS2 shows a lattice spacing of 0.230 nm (Fig. 2c), corresponding to the (111) planes of the AuAg alloy, which has nearly the same crystalline structure as Au or Ag (fcc). Fig. 2d shows a lattice spacing of 0.303 nm in Ag_2S part, corresponding to the presence of (111) planes of Ag_2S.

The composition of as prepared HS2 product was further investigated by X-ray photoelectron spectroscopy (XPS), as shown in Fig. S5. The survey spectrum in Fig. S5a indicates Au, Ag and S elements, as well as O and C, which came from organic molecules on the surface. Furthermore, the absence of a Zn signal confirms that the ZnS NRs had been completely converted into Ag_2S nanotubes in HS2, which is consistent with the result of XRD. Meanwhile, the XPS data shows that the stoichiometric ratio of Au:Ag:S is 9:6:1. The measured atomic ratio of Ag:S (6:1) in the heterostructures is much higher than the stoichiometric ratio of 2:1 for Ag_2S. Therefore, the particles tipping on the tubes are confirmed to be AuAg alloy

rather than pure Au, which is consistent with the results of EDX line-scanning analysis. The molar ratio of Ag element in the alloy to that in Ag_2S was calculated to be 2:1, and the ratio of Au to Ag in the alloy was 9:4. Therefore, the molar ratio of gold to Ag (0) to Ag_2S is approximately 9:4:1 in the preapred heteronanostructure. Fig. 4sb displays a high-resolution XPS pattern of Au, showing 4f peaks at 84.0 eV and 87.6.0 eV.[14] Fig. 4sc shows the Ag 3d binding energy that yielded two sets of peaks. The peaks at 373.9 eV and 367.8 eV correspond, respectively, to binding energies of $3d_{3/2}$ and $3d_{5/2}$ of metallic Ag (0).[15] The peaks located at 373.4 eV and 367.4 eV are attributed to binding energies of $3d_{3/2}$ and $3d_{5/2}$ of Ag (I).[16] The molar ratio of Ag (0) to Ag (I) was calculated to be 2.1:1 based on their respective peak areas. This ratio is in good accordance with the above molar ratio of Ag element in the AuAg alloy to that in Ag_2S. The XPS data of Fig. 4sd shows the binding energy of S 2p; the deconvoluted binding energies of 161.1 eV and 162.1 eV can be assigned to S $2p_{3/2}$ and S $2p_{1/2}$, indicating the presence of S^{2-}.

The process and mechanism of HS1 transferring to HS2 were investigated in this work. The ~5 nm diameter of AuAg alloy nanoparticles in HS2 was larger than that of gold nanoparticles in HS1 (~2 nm). So we believed that the AuAg alloy nanoparticles formed by ripening growth of gold nanoparticles with Ag^+ in the solution. On the other hand, the evolution from ZnS NR to Ag_2S QT is believed to be driven by Kirkendall effect, which has produced many hollow nanostructures.[17] It means that atomic diffusion occurs through vacancy exchange (not the direct interchange of atoms) at a solid/gas or solid/liquid interface, leading to the hollow nanostructure. Here, the Ag^+ ions adsorbed on the NRs surface, and reacted with ZnS to form an Ag_2S thin layer, made possible because Ag_2S is much more stable than ZnS. The inner S^{2-} ions in the ZnS NRs were separated from the outside Ag^+ in the bulk solution due to the Ag_2S thin layer, which blocked direct cation exchange between Ag^+ and ZnS. However, the Ag^+ ions diffused inward to react further with the outward S^{2-} ions to form Ag_2S at the solid/liquid interface motivated by the Kirkendall effect, resulting in a void formation in ZnS NR. Scheme 1b depicts the top-view of ZnS NR along the axial direction. There are only two or three layers of ZnS in the range of their ultrasmall diameter. Thus, S^{2-} diffusion from the inner layers to the surface of ZnS NR occurs quickly through vacancy exchange (Kirkendall effect) for the ultrashort diffusion distance. This intermediate mechanism is illustrated in Scheme 1c.

The important feature of the heteronanostructure is the electronic coupling between the metal and semiconductor domains. To investigate this feature, the UV-visible and photoluminescence (PL) spectra of the obtained HS2 in cyclohexane at room temperature were characterized. Fig. S6a shows the UV−visible absorption of the HS2 product. The absorption increased intensely in the shorter wavelengths (< 600 nm), coinciding with those of previously reported Ag_2S QDs.[11a, 12a] It means that the HS2 sample has a good absorption for visible light with the wavelength less than 600 nm. Simultaneously, the surface plasmon resonance (SPR) from the AuAg alloy part in the heterostructure was not detected in the UV-visible spectrum. According to a previous study, the SPR peak of the AuAg alloy nanoparticles with a ratio of 9:4 was calculated to locate at approximately 490 nm.[18] The missing of SPR peak from absorption spectrum of HS2 indicates that the nature of excited electron oscillations in ally domains is modified due to direct coupling of Ag_2S QTs.[19] Fig. S6b shows the HS2 product emitted NIR luminescence at approximately 952 nm by the excitation of 470 nm, as shown in Fig. S6b. This NIR emission agrees well with the characterized luminescence of Ag_2S QDs. However, the emission peak at 952 nm (1.30 eV) indicates an obvious blue shift compared to Ag_2S bulk materials and QDs.[12a, 12b] This was attributed to the strong quantum confined effect of the ultrathin shells of the Ag_2S QTs. The lifetime of their PL emission is approximately 0.8 μs as shown in inset of Fig. S6b. This value of lifetime is much longer than that of reported Ag_2S QDs (57-181 ns),[12a] which also illustrates the electronic coupling between AuAg alloy and Ag_2S.

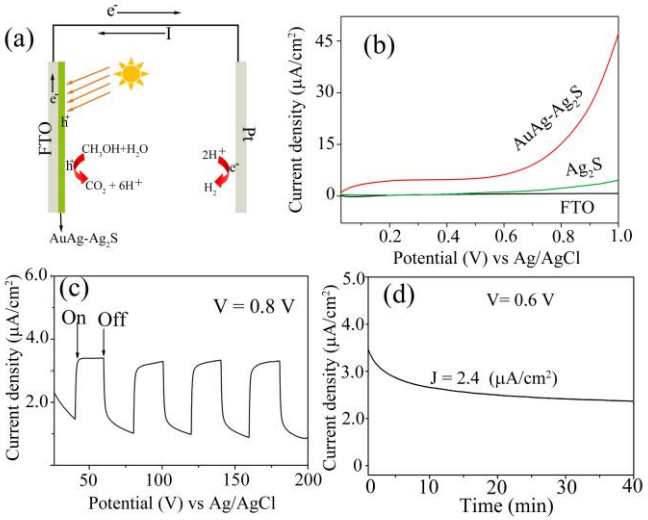

Fig. 3. Scheme of the electron–hole pair separation and transfer process as well as electrode reactions in the PEC test (a); The linear voltammogram (LSV) curves under visible light illumination for defferent samples, as denoted (b). The corresponding amperometric *J-t* curve under light switching on and off at the applied potential of 0.8 $V_{Ag/AgCl}$ (c). Photocurrent density versus time (*J-t*) curves of the obtained HS2 product photoanode performed at 0.6 $V_{Ag/AgCl}$.

The metal-semiconductor heteronanostructures were attractive for energy conversion applications owing to their charge separation effect. Here, the prepared HS2 nanostructure was examined for their PEC catalysis actives for the H_2 generation reaction. The PEC performance of the sample was tested in 1.0 M methanol electrolyte by a conventional three-electrode system under irradiation of 350 W Xe lamp with a filter (λ> 400 nm). As an electron donor, methanol can be oxided by holes because the standard electrode potential of $E_{H2CO3/CH3OH}$ (+0.04V) is more negative than that for reduction of $E_{O2/H2O}$ (+1.23 V).[20] The applied potential on PEC drives the photogenerated electrons to drift towards the Pt counter electrode, where the H_2 evolution occurs. The PEC process is schemed in Fig. 3a. The chemical reaction equations in the presence of methanol can be expressed as follows:

$$\text{Anode}: CH_3OH + H_2O + 6h^+ \rightarrow CO_2 + 6H^+ \quad (1)$$

$$\text{Cathode}: 6H^+ + 6e^- \rightarrow 3H_2 \quad (2)$$

Fig. 3b displays the FTO substrate responded a quite weak dark current density at a bias potential of 1.0 V vs AgCl/Ag. However, the obtained HS2 sample on FTO electrode exhibited a much enhanced photocurrent density of 44.6 μA cm^{-2} under visible light irradiation. It should be pointed out that this result was achieved by the sample that was coated by organic surfactant moleculers on their surface, which would prevent partial light absorption and charge transfer between the materials and FTO substrate. As a comparison, Ag_2S nanotubes were prepared (Fig. S8, see ESI) and tested for PEC activity. The photocurrent density of Ag_2S nanotubes was 3.4 μA cm^{-2} at 1.0 V vs Ag/AgCl (Fig. 3b), much smaller than that of HS2. This result indicates the coupling occurred in HS2 and it enhanced photoelectrocatalytic activity of HS2. The corresponding transient photocurrent density vs time (*J-t*) curves of the HS2 sample electrode measured under light illumination with 20s light ON/Off

cycles are displayed in Fig. 3c. It can be seen that the HS2 sample had good photo-switching performance with fast response time and stable photostability. The chemical stability against anodic photo-oxidation is important to photoanode materials. Fig. 3d displays the *J-t* curve of HS2 at a constant potential of 0.6V vs AgCl/Ag under illumination for 40 min. The results show that the obtained HS2 sample had high stability in PEC photocatalysis of H_2 evolution.

In summary, we have demonstrated the synthesis of gold-silver alloy tipped on Ag_2S QTs heterostructure using a two-step method. It was considered that the Kirkendall effect was responsible for the formation of the Ag_2S QT composite, and Au nanoparticles ripening with Ag^+ were responsible for the formation of AuAg alloy nanoparticles. The optical properties of the heterostructures were characterized using by UV-visible and PL spectroscopy, which displayed the electronic coupling between metal part and semiconductor part. Furthermore, the prepared novle AuAg-Ag_2S heteronanostructure also displayed stable and effective PEC catalytic H_2 evolution.

We thank NSFC (51402201); Beijing Youth Talent (CIT&TCD201404162); Beijing Local College Innovation Team Improve Plan (IDHT20140512); Scientific Research Base Development Program of the Beijing Municipal Commission of Education.

Notes and references

Department of Chemistry, Beijing Key Laboratory for Optical Materials and Photonic Devices, Capital Normal University, Beijing, 100048, P. R. China.
Email: tianyang@cnu.edu.cn
Electronic Supplementary Information (ESI) available: Experimental section, supplementary Fig.s. See DOI: 10.1039/c000000x/

1 (a) R. Jiang, B. Li, C. Fang and J. Wang, *Adv. Mater.*, 2014, **26**, 5274; (b) A. Demortiere, R. D. Schaller, T. Li, S. Chattopadhyay, G. Krylova, T. Shibata, P. C. dos Santos Claro, C. E. Rowland, J. T. Miller, R. Cook, B. Lee and E. V. Shevchenko, *J .Am .Chem. Soc.*, 2014, **136**, 2342; (c) U. Banin, Y. Ben-Shahar and K. Vinokurov, *Chem. Mater.*, 2013, **26**, 97; (d) R. Costi, A. E. Saunders and U. Banin, *Angew. Chem. Int. Ed.*, 2010, **49**, 4878; (e) L. Carbone, A. Jakab, Y. Khalavka and C. Sönnichsen, *Nano Lett.*, 2009, **9**, 3710.

2 (a) Z. Huang, M. Li, D. Jia, P. Zhong, F. Tian, Z. Chen, M. G. Humphrey and C. Zhang, *J. Mater. Chem. C*, 2014, **2**, 1418; (b) P. Yu, X. Wen, Y.-C. Lee, W.-C. Lee, C.-C. Kang and J. Tang, *J. Phys. Chem. Lett.*, 2013, **4**, 3596; (c) D. Mongin, E. Shaviv, P. Maioli, A. Crut, U. Banin, N. Del Fatti and F. Vallée, *ACS Nano*, 2012, **6**, 7034.

3 (a) U. Soni, P. Tripathy and S. Sapra, *J. Phys. Chem. Lett.*, 2014, **5**, 1909; (b) L. Wang, J. Ge, A. Wang, M. Deng, X. Wang, S. Bai, R. Li, J. Jiang, Q. Zhang, Y. Luo and Y. Xiong, *Angew. Chem. Int. Ed.*, 2014, **53**, 5107; (c) X. Yu, A. Shavel, X. An, Z. Luo, M. Ibáñez and A. Cabot, *J. Am. Chem. Soc.*, 2014, **136**, 9236; (d) Q. Lu, Z. Lu, Y. Lu, L. Lv, Y. Ning, H. Yu, Y. Hou and Y. Yin, *Nano Lett.*, 2013, **13**, 5698; (e) I. Hamada, R. Shimizu, T. Ohsawa, K. Iwaya, T. Hashizume, M. Tsukada, K. Akagi and T. Hitosugi, *J. Am. Chem. Soc.*, 2014; (f) X. Hong, Z. Yin, Z. Fan, Y.-Y. Tay, J. Chen, Y. Du, C. Xue, H. Chen and H. Zhang, *Small*, 2014, **10**, 479; (g) L. Xu, Z. Yin, S.-W. Cao, Z. Fan, X. Zhang, H. Zhang and C. Xue, *Chemistry – A European Journal*, 2014, **20**, 2742.

4 (a) S.-U. Lee, J. W. Hong, S.-I. Choi and S. W. Han, *J. Am. Chem. Soc.*, 2014, **136**, 5221; (b) Z. W. Seh, S. Liu, M. Low, S.-Y. Zhang, Z. Liu, A. Mlayah and M.-Y. Han, *Adv. Mater.*, 2012, **24**, 2310.

5 (a) G. Menagen, J. E. Macdonald, Y. Shemesh, I. Popov and U. Banin, *J. Am. Chem. Soc.*, 2009, **131**, 17406; (b) J. Maynadié, A. Salant, A. Falqui, M. Respaud, E. Shaviv, U. Banin, K. Soulantica and B. Chaudret, *Angew. Chem. Int. Ed.*, 2009, **48**, 1814; (c) A. E. Saunders, I. Popov and U. Banin, *J. Phys. Chem. B*, 2006, **110**, 25421.

6 H. Schlicke, D. Ghosh, L.-K. Fong, H. L. Xin, H. Zheng and A. P. Alivisatos, *Angew. Chem. Int. Ed.*, 2013, **52**, 980.

7 (a) Y. Kim, K. Y. Park, D. M. Jang, Y. M. Song, H. S. Kim, Y. J. Cho, Y. Myung and J. Park, *J. Phys. Chem. C*, 2010, **114**, 22141; (b) M. Pang, J. Hu and H. C. Zeng, *J. Am. Chem. Soc.*, 2010, **132**, 10771; (c) P. Li, Z. Wei, T. Wu, Q. Peng and Y. Li, *J. Am. Chem. Soc.*, 2011, **133**, 5660; (d) S. Xiong, B. Xi, K. Zhang, Y. Chen, J. Jiang, J. Hu and H. C. Zeng, *Sci. Rep.* 2013, **3**, 2177.

8 (a) H. T. Chung, J. H. Won and P. Zelenay, *Nat Commun*, 2013, **4**, 1922; (b) C. Liu, Y. Y. Fan, M. Liu, H. T. Cong, H. M. Cheng and M. S. Dresselhaus, *Science*, 1999, **286**, 1127; (c) G. Che, B. B. Lakshmi, E. R. Fisher and C. R. Martin, *Nature*, 1998, **393**, 346; (d) K.-S. Cho, D. V. Talapin, W. Gaschler and C. B. Murray, *J. Am. Chem. Soc.*, 2005, **127**, 7140.

9 (a) J. Han, Z. Liu, K. Guo, B. Wang, X. Zhang and T. Hong, *Appl. Catal., B*, 2015, **163**, 179; (b) P. Roy, S. Berger and P. Schmuki, *Angew. Chem. Int. Ed.*, 2011, **50**, 2904.

10 (a) W. P. Lim, Z. Zhang, H. Y. Low and W. S. Chin, *Angew. Chem. Int. Ed.*, 2004, **43**, 5685; (b) Y.-P. Sun, J. E. Riggs, H. W. Rollins and R. Guduru, *J. Phys. Chem. B*, 1998, **103**, 77.

11 (a) G. Hong, J. T. Robinson, Y. Zhang, S. Diao, A. L. Antaris, Q. Wang and H. Dai, *Angew. Chem. Int. Ed.*, 2012, **51**, 9818; (b) P. S. Nikam and C. B. Shinde, *Pramana*, 1994, **43**, 55; (c) G. Hodes, J. Manassen and D. Cahen, *Nature*, 1976, **261**, 403.

12 (a) Y. Zhang, Y. Liu, C. Li, X. Chen and Q. Wang, *J. Phys. Chem. C*, 2014, **118**, 4918; (b) Y. Zhang, G. Hong, Y. Zhang, G. Chen, F. Li, H. Dai and Q. Wang, *ACS Nano*, 2012, **6**, 3695; (c) J. Li, W. Yang, J. Ning, Y. Zhong and Y. Hu, *Nanoscale*, 2014, **6**, 5612; (d) D. Wang, C. Hao, W. Zheng, Q. Peng, T. Wang, Z. Liao, D. Yu and Y. Li, *Adv. Mater.*, 2008, **20**, 2628; (e) X. Wen, S. Wang, Y. Xie, X.-Y. Li and S. Yang, *J. Phys. Chem. B*, 2005, **109**, 10100; (f) J. Xiang, H. Cao, Q. Wu, S. Zhang, X. Zhang and A. A. R. Watt, *J. Phys. Chem. C*, 2008, **112**, 3580; (g) X. Fu, H. Zou and L. Zhou, *J. Nanosci. Nanotech.*, 2010, **10**, 5851.

13 J. Yang and J. Y. Ying, *Angew. Chem. Int. Ed.*, 2011, **50**, 4637.

14 W. S. Epling, G. B. Hoflund, J. F. Weaver, S. Tsubota and M. Haruta, *J. Phys. Chem.*, 1996, **100**, 9929.

15 J. C. Fuggle, E. Kälne, L. M. Watson and D. J. Fabian, *Phys. Rev. B*, 1977, **16**, 750.

16 Y. Du, B. Xu, T. Fu, M. Cai, F. Li, Y. Zhang and Q. Wang, *J. Am. Chem. Soc.*, 2010, **132**, 1470.

17 (a) L. Shi and Y. Dai, *J. Mater. Chem. A*, 2013, **1**, 12981; (b) Z. Fei, S. He, L. Li, W. Ji and C.-T. Au, *Chem. Commun.*, 2012, **48**, 853.

18 M. P. Mallin and C. J. Murphy, *Nano Lett.*, 2002, **2**, 1235.

19 (a) E. Khon, A. Mereshchenko, A. N. Tarnovsky, K. Acharya, A. Klinkova, N. N. Hewa-Kasakarage, I. Nemitz and M. Zamkov, *Nano Lett.*, 2011, **11**, 1792; (b) A. K. Geim and K. S. Novoselov, *Nat Mater*, 2007, **6**, 183.

20 T. Hisatomi, J. Kubota and K. Domen, *Chem. Soc. Rev.*, 2014, **43**, 7520.

